REVIEW / SYNTHÈSE

Tungsten spectroscopy at the Livermore electron beam ion trap facility[1]

J. Clementson, P. Beiersdorfer, G.V. Brown, M.F. Gu, H. Lundberg, Y. Podpaly, and E. Träbert

Abstract: The utilization of tungsten spectroscopy for diagnostics of magnetically confined fusion plasmas requires the radiative properties of tungsten ions to be accurately known. At the Lawrence Livermore National Laboratory, a program to gather spectroscopic data on tungsten ions has been initiated with the purpose to study spectral signatures and identify candidate fusion plasma diagnostics. In this paper, an overview of recent results from the Livermore WOLFRAM spectroscopy project is presented, which includes experimental investigations at the EBIT-I and SuperEBIT electron beam ion traps. In particular, the spectra of highly charged M- and L-shell tungsten ions have been studied. These investigations cover energy measurements of $n = 2$ to $n = 2$, 3 transitions in Ne-like W^{64+} through Li-like W^{71+} ions and soft X-ray measurements of $n = 3$ to $n = 3$, 4 transitions in M-shell ions with emphasis on the Ni-like W^{46+} and Si-like W^{60+} through Na-like W^{63+} ions. The measurements are complemented by atomic-structure calculations and spectral modeling using the Flexible Atomic Code (FAC).

PACS Nos: 32.30.Rj, 52.70.La, 52.72.+v, 52.25.Vy, 31.15.am

Résumé : L'utilisation de la spectroscopie du tungstène dans les diagnostiques de plasmas de fusion confinés magnétiquement exige de connaître avec précision les propriétés radiatives des ions de tungstène. Au Lawrence Livermore National Laboratory, nous avons démarré un programme pour amasser des données spectroscopiques sur les ions de tungstène, afin d'étudier les signatures spectrales et d'identifier les candidats pouvant servir à diagnostiquer les plasmas de fusion. Nous passons ici en revue les récents résultats du projet de spectroscopie WOLFRAM de Livermore, incluant les mesures expérimentales avec les pièges ioniques à faisceau d'électrons EBIT-I et SuperEBIT. Nous avons étudié en particulier les spectres des couches L et M d'ions fortement chargés. Ces mesures couvrent les transitions $n = 2$ à $n = 2$, 3 dans les ions tungstène de type Ne, W^{64+}, jusqu'aux ions de type Li, W^{71+}, ainsi que les rayons-X mous des transitions de $n = 2$ vers $n = 3$, 4 dans la couche M, en insistant sur les ions de type Ni, W^{46+} et de type Si, W^{60+}, jusqu'au type Na, W^{63+}. Les mesures sont présentées avec des calculs de structure atomique et de modélisation spectrale utilisant le « Flexible Atomic Code » (FAC).

[Traduit par la Rédaction]

1. Introduction

The radiative properties of tungsten ions need to be better known to fully take advantage of the opportunities tungsten spectra offer for high-temperature fusion plasma diagnostics. With seventy-five charge states, tungsten emission could exist over a very wide range of plasma conditions. Most of the ions have complex atomic structure, making tungsten spectra observed in magnetic fusion plasmas challenging to interpret. Neutral and few-times ionized tungsten have been extensively studied in the optical and ultraviolet regions [1–5]. Medium-charge tungsten ions have been observed in tokamak plasmas since the 1970s [6–10], but the complex transition arrays have then mostly been seen as unresolved quasi continua making individual ions difficult to identify. Yet higher charge states have been studied in laser-produced plasmas, tokamaks, and at electron beam ion traps (EBITs), where several high-precision measurements have been performed [11–15]. Highly charged tungsten ions are furthermore of interest for atomic theory, because effects on the atomic structure from

Received 8 October 2010. Accepted 22 November 2010. Published at www.nrcresearchpress.com/cjp on 20 May 2011.

J. Clementson, P. Beiersdorfer, G.V. Brown, and E. Träbert. Lawrence Livermore National Laboratory, Livermore, CA 94550, USA.
M.F. Gu. University of California, Berkeley, CA 94720, USA.
H. Lundberg. Lund University, SE-221 00 Lund, Sweden.
Y. Podpaly. MIT Plasma Science and Fusion Center, Cambridge, MA 02139, USA.

Corresponding author: J. Clementson (e-mail: clementson@llnl.gov).

[1]This review is part of a Special Issue on the 10th International Colloquium on Atomic Spectra and Oscillator Strengths for Astrophysical and Laboratory Plasmas.

quantum electrodynamics (QED) and relativity can be studied and used to benchmark large-scale calculations. Nevertheless, it is the return of tungsten as a construction material in magnetic confinement fusion devices that is the driving force for tungsten spectroscopy. Tungsten is of interest due to excellent thermal properties, making it very attractive for plasma-facing surfaces that are expected to receive high heat loads. It has the highest melting point of non-alloyed metals, a high-energy sputtering threshold, and low tritium retention [16–18]. Several present-day tokamaks are now operating with, or are planning to install, tungsten parts. In the ITER tokamak, the divertor target plates will be made of tungsten. Despite its favorable properties, it is still likely that tungsten particles will sputter off the surfaces and get introduced into the divertor plasmas. The ions can then be transported into the plasma core where the high temperatures will lead to further ionization of the particles. Tungsten has sufficiently high nuclear charge Z to prevent the complete stripping of the electrons and will thus emit line radiation even in the hottest part of a fusion device. Too large concentrations of tungsten ions in a reactor could then radiatively cool the plasma enough to prevent fusion burn conditions to be reached. At the same time, the incompletely stripped tungsten ions can also act as probes of the plasma interior, relaying information about the plasma conditions. This, then, requires the spectra of tungsten to be accurately known under a variety of plasma conditions. This includes the spectra of few-times ionized tungsten that can be found in the cooler parts of the plasma, such as the divertor and edge plasmas, as well as medium- to high-charge tungsten ions that will be created in the hotter parts of the plasma.

Several spectroscopic measurements on highly charged tungsten ions have been carried out during the last few years. Most of these studies have been performed on electron beam ion traps, mainly at the Lawrence Livermore National Laboratory [19–22], Berlin [17, 23–26], and the National Institute of Standards and Technology (NIST) [27–30] EBIT facilities, as well as at the ASDEX upgrade tokamak [15, 16, 31].

2. The WOLFRAM project

To address the need for spectroscopic data on tungsten, the WOLFRAM project has been initiated at the Lawrence Livermore National Laboratory in Livermore, California. The purpose of the program is to measure atomic spectra from few-times ionized to highly charged tungsten ions and to develop tungsten-based plasma diagnostics for magnetic fusion research.

Atomic spectra often need to be known both in broad band and in high resolution. Wide spectral surveys are useful for the identification of emission from individual charge states, whereas high-resolution measurements allow for a variety of high-precision diagnostics, such as electron-density, plasma-flow, and ion-temperature measurements. For spectroscopic investigations of tungsten ions, the Livermore EBIT facility is well equipped. With two electron beam ion traps to create, confine, and excite tungsten ions and an extensive suite of spectroscopic instrumentation, covering the optical to X-ray regions, most tungsten spectra can be studied. The original electron beam ion trap, EBIT-I, has been in operation in Livermore since 1986 [32–34]. It can be operated at electron-beam energies up to 30 keV with beam currents above 200 mA. The high-voltage upgrade device, known as Super-EBIT, was built in 1992 and can run experiments at energies in excess of 200 keV [35].

In the EBIT trap region, where the electron beam is compressed to electron densities of around 10^{11}–10^{12} cm^{-3}, ions are trapped radially by the negative space charge. A set of drift-tube electrodes keeps the ions from escaping in the axial direction along the beam. The drift-tube assembly of the Livermore EBIT has six radial ports surrounding the electromagnetic trap, so that spectrometers, detectors, and material injectors can be mounted close to the trap. Depending on the material, a variety of methods exist to introduce the atoms, molecules, or ions into EBIT. For tungsten, a metal vapor vacuum arc (MeVVA) can be used, which sputters tungsten ions off from an electrode located on the top of EBIT. Tungsten can also be brought into the trap by sublimation of the crystalline compound tungsten hexacarbonyl, $W(CO)_6$, letting the molecules diffuse into the EBIT vacuum chamber. When the injected particles reach the trap, collisions with the beam electrons will ionize and excite them. The energy of the electron beam determines the charge balance of the trap plasma. To observe the emitted radiation from the trap, a large number of crystal and grating spectrometers have been designed and built at the Livermore EBIT facility [36–41]. These instruments allow for broad surveys and high-resolution measurements of EUV and X-ray emissions. A fruitful collaboration with the NASA Goddard Space Flight Center has resulted in the implementation of several X-ray calorimeter spectrometers at Livermore [42]. X-ray calorimeters (also known as microcalorimeters and quantum calorimeters [43]) are under rapid development and have proven very useful for broad-band surveys. The spectrometers operate in event mode, and with moderate resolution the instruments have proven ideal for plasma diagnostics and for the study of highly charged ions at the Livermore EBIT. The connection of X-ray calorimeters and EBIT has initiated the founding of the Fusion and Astrophysics (FAST) facility at Livermore. FAST is a user facility that allows external collaborators to test and calibrate spectroscopic diagnostics for laboratory and astrophysical plasmas [44].

Highly charged tungsten ions have been studied at the Livermore EBIT facility since the early 1990s, when Beiersdorfer measured wavelengths in sixty-four times ionized neon-like tungsten for isoelectronic studies of level crossings [45]. Elliott and Beiersdorfer et al. measured a resonance transition in forty-six times ionized nickel-like tungsten of interest in X-ray laser research [46, 47]. Utter et al. studied $n = 4$ to $n = 4$ transitions in Rb-like W^{37+} through Cu-like W^{45+} [20], and also an optical M1 transition in Ti-like W^{52+} [19]. Moreover, Neill et al. [21] and Safronova et al. [22] have studied M-shell spectra from ions around nickel-like tungsten.

In addition to atomic physics studies of tungsten ions, the WOLFRAM project includes plasma spectroscopy of tungsten and the development of novel fusion plasma diagnostics. Such measurements have been performed at the Sustained Spheromak Physics Experiment (SSPX), a small-scale innovative confinement concept project in Livermore, in operation from 1999 to 2007. The main objectives of the SSPX spheromak were the study of energy confinement and mag-

Fig. 1. Tungsten ionization balance calculated for $n_e = 10^{14}$ cm^{-3}. Fractional abundances for the M-shell ions (ions with $n = 3$ ground configurations) are displayed in red (dark grey in print version). These ions include Ni-like W^{46+} through Na-like W^{63+}. L-shell ions (ions with $n = 2$ ground configurations) are displayed in blue (light grey in print version) and include Ne-like W^{64+} through Li-like W^{71+}. Of the K-shell ions (ions with $n = 1$ ground configurations), only He-like W^{72+} has a fractional abundance above 1% for electron temperatures below 50 keV.

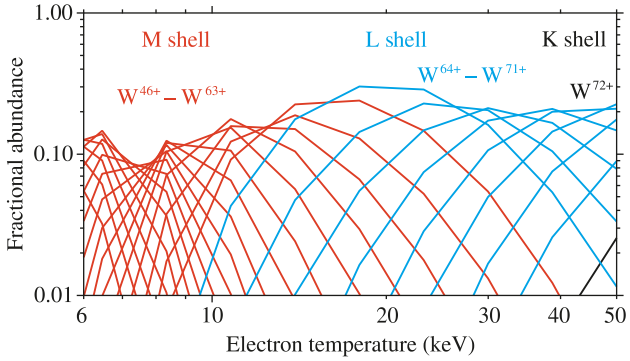

Fig. 2. Top: Experimental spectrum of tungsten measured at EBIT-I using the ECS spectrometer at an electron-beam energy of $E_b = 6.5$ keV. Middle: Theoretical spectrum of tungsten calculated using FAC. Bottom: Theoretical spectra calculated using FAC displaying the tungsten charge states. Spectra are labeled according to isoelectronic sequence. Figure is adapted from [77].

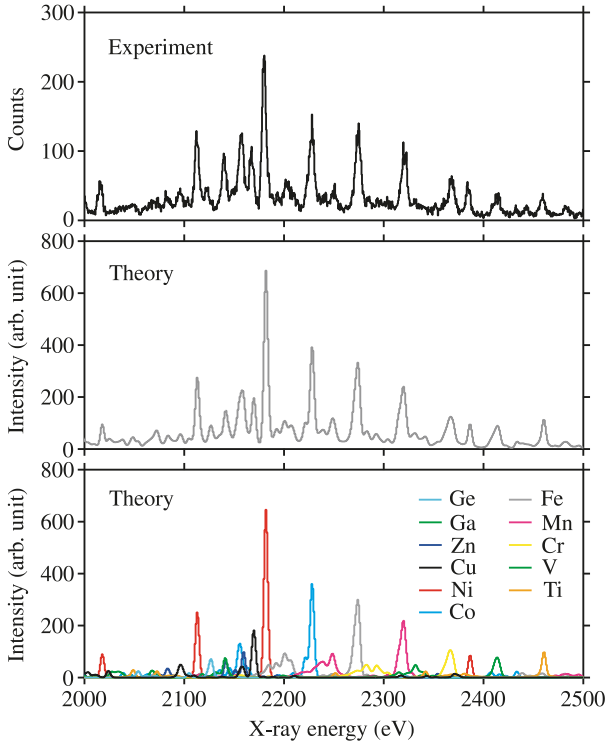

netic field build-up in spheromak plasmas. However, the spheromak also proved very useful for spectroscopic investigations [48]. Tungsten was injected into SSPX plasmas by the sublimation of tungsten hexacarbonyl, with the purpose to simulate the emission from ITER divertor plasmas. The plasma conditions of the SSPX spheromak much resembled

Fig. 3. Calculated Gaussian line profiles for the two nickel-like tungsten lines E2 and M3 for electron and ion temperatures of 1, 3, 5, and 7 keV and for electron densities of 1×10^{13} and 1×10^{14} cm^{-3}. Figure is adapted from [77].

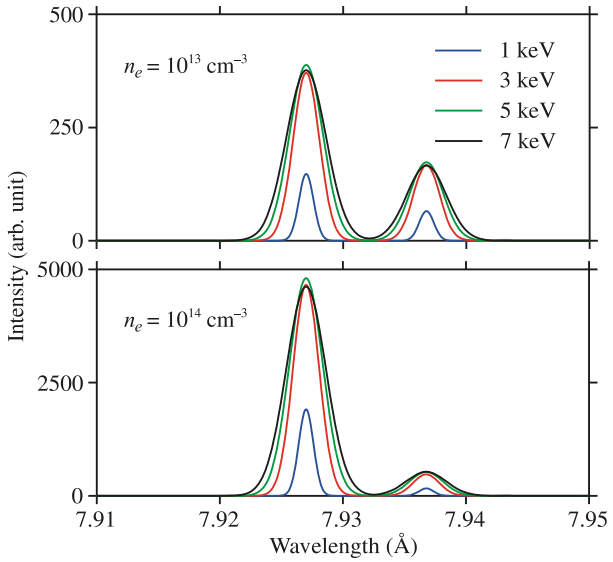

Fig. 4. Theoretical tungsten spectra calculated for $n_e = 1 \times 10^{14}$ cm^{-3} for $T_e = T_i = 10$, 20, and 30 keV. Strong lines are labeled according to charge state. Figure is adapted from [77].

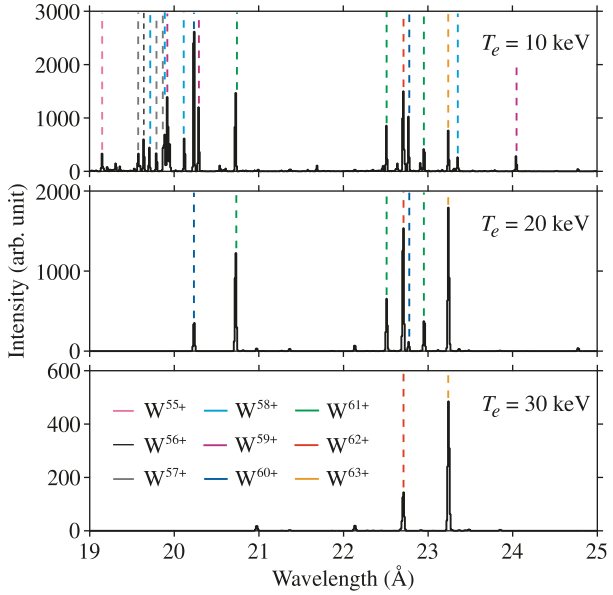

those expected in the ITER divertor, with electron densities around 10^{14}–10^{15} cm^{-3} and electron temperatures below 200 eV [49]. The WOLFRAM project also includes work at external facilities, such as the MIT Alcator C-Mod tokamak [50, 51] and the Princeton NSTX tokamak [52].

To guide and complement tungsten measurements, atomic-structure calculations and spectral modeling are performed, mostly using the Flexible Atomic Code (FAC). FAC is a fully relativistic atomic physics package based on the Dirac equation. It was written and developed by Gu [53]. QED effects are included with the Breit interaction in the zero energy limit for the exchanged photon, and hydrogenic approximations for self-energy and vacuum polarization ef-

Table 1. Experimental and theoretical wavelengths for resonance transitions in Si-like W^{60+}, Al-like W^{61+}, Be-like W^{70+}, and Li-like W^{71+} ions.

Ion	Transition	Experiment (Å)	Theory (Å)
Si-like W^{60+}	$(3s^23p_{1/2}^2)_0$–$(3s^23p_{1/2}3d_{3/2})_1$	20.270(5)[a]	20.26343[b]
		20.26(2)[c]	
Al-like W^{61+}	$(3s^23p_{1/2})_{1/2}$–$(3s^23d_{3/2})_{3/2}$	20.756(4)[a]	20.73730[d]
		20.72(2)[c]	20.7684[e]
Ion	Transition	Experiment (eV)	Theory (eV)
Be-like W^{70+}	$(2s^2)_0$–$(2s_{1/2}2p_{3/2})_1$	1741.4(6)[f]	1740.538[e]
		1741(1)[g]	1741.47[h]
			1741.371[i]
Li-like W^{71+}	$(2s_{1/2})_{1/2}$–$(2p_{3/2})_{3/2}$	1696.2(5)[f]	1695.9946[j]
		1697(1)[g]	1696.0309[k]
			1695.42[l]

[a]Clementson and Beiersdorfer [78]
[b]Huang [79]
[c]Gillaspy et al. [30]
[d]Huang [80]
[e]Safronova and Safronova [81]
[f]Clementson [77]
[g]Podpaly et al. [85]
[h]Chen and Cheng [86]
[i]Safronova et al. [87]
[j]Kim et al. [88]
[k]Chen et al. [89]
[l]Safronova et al. [90]

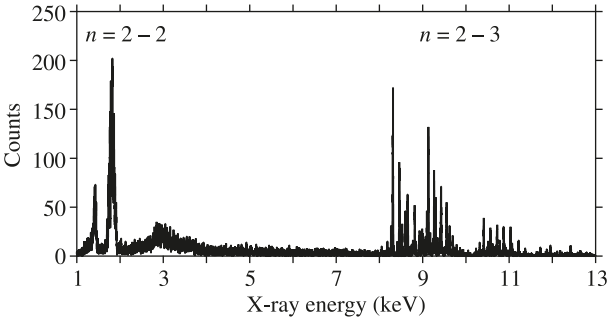

Fig. 5. Survey spectrum of L-shell tungsten ions taken at SuperEBIT with the ECS spectrometer at an electron-beam energy of E_b = 51 keV. Figure is adapted from [77].

fects. Theoretical support is also provided by the atomic physics group at the University of Nevada at Reno [54, 55].

In this paper, an overview is given of recent spectroscopic measurements of tungsten carried out at the Livermore EBIT facility under the WOLFRAM project. The experiments presented here have focused on wavelength and transition-energy measurements of M- and L-shell tungsten ions. These charge states are particularly important for high-temperature plasmas expected in the next generation fusion devices, such as ITER core plasmas, where the electron and ion temperatures are predicted to exceed 30 keV under certain operation scenarios [56]. Figure 1 displays the tungsten ionization balance calculated for a typical tokamak plasma. Unit conversions used throughout the paper are hc = 12 398.42 Å eV = 1/8065.5410 eV cm, and 1 Ry = 13.605 69 eV. The uncertainties given in the tables and text of the present article represent the statistical and systematic uncertainties combined in quadrature.

3. M-shell tungsten spectroscopy

Several M-shell tungsten spectra have been investigated within the WOLFRAM project, both experimentally and theoretically. Continuing the studies of Neill et al. [21] and Safronova et al. [22] on the soft X-ray spectra of around forty-six times ionized tungsten, broad-band measurements have been performed using X-ray calorimeters on EBIT-I and SuperEBIT. One of these measurements focused on transitions from Zn-like W^{44+} through Co-like W^{47+}, made with the X-ray spectrometer (XRS) instrument [42] on SuperEBIT, which was operated at electron-beam energies of E_b = 3.3, 4.0, and 4.1 keV [57]. Tungsten lines were measured in the 1500–3600 eV interval, thereby covering M-shell transitions with upper levels from n = 4 to n = 8. A number of new lines were measured in addition to the improvement of the accuracies of previously measured transition energies.

This study was followed by higher electron-beam energy measurements using the EBIT calorimeter spectrometer (ECS) instrument [58–60] at EBIT-I, which focused on the Δn = 1 transitions in the 2000–2500 eV interval. EBIT-I was operated at energies from 4.0 to 6.5 keV to create higher charge states than those studied in [57]. Tungsten was supplied to the trap by sublimation of tungsten hexacarbonyl, and the spectra were energy calibrated using the K-shell emission from neon and argon ions. Tungsten line identification was supported by FAC calculations. The spectra of Ge-like W^{42+} through Ti-like W^{52+} were modeled for EBIT plasma conditions. Spectral line widths were set to 4.5 eV, which corresponds to the experimental resolution of the ECS instrument. Theoretical spectra are shown in Fig. 2 together with an experimental spectrum. The charge balance in the trap was estimated from the measured line intensities and the calculated line emissivities. The relative abundances of Ga-

Table 2. Tungsten $\Delta n = 0$ L-shell transition energies.

Line	Lower level	Upper level	Calorimeter	Crystal	Theory
B-3	$(2s_{1/2}2p^2_{1/2})_{1/2}$	$(2s^22p_{3/2})_{3/2}$	1192.5(6)		1191.6
F-2	$(2s^22p^2_{1/2}2p^3_{3/2})_{3/2}$	$(2s^22p_{1/2}2p^4_{3/2})_{1/2}$	1388.9(6)		1389.8
C-2	$(2s^22p^2_{1/2})_0$	$(2s^22p_{1/2}2p_{3/2})_2$	1429.7(5)		1430.4
Ne-1	$(2s^22p^2_{1/2}2p^3_{3/2}3s_{1/2})_1$	$(2s^22p_{1/2}2p^4_{3/2}3p_{1/2})_0$	1570.7(8)		1573.2
B-2	$(2s^22p_{1/2})_{1/2}$	$(2s_{1/2}2p_{1/2}2p_{3/2})_{3/2}$	1654.0(6)		1654.6
Li-1	$(2s_{1/2})_{1/2}$	$(2p_{3/2})_{3/2}$	1696.2(5)	1697(1)	1697.7
N-2	$(2s^22p^2_{1/2}2p_{3/2})_{3/2}$	$(2s_{1/2}2p^2_{1/2}2p^2_{3/2})_{5/2}$	1733.9(8)	1734(1)	1735.6
Be-1	$(2s^2)_0$	$(2s_{1/2}2p_{3/2})_1$	1741.4(6)	1741(1)	1744.2
B-1a	$(2s^22p_{1/2})_{1/2}$	$(2s_{1/2}2p_{1/2}2p_{3/2})_{1/2}$		1767(1)	1769.7
B-1b	$(2s^22p_{1/2})_{1/2}$	$(2s_{1/2}2p_{1/2}2p_{3/2})_{3/2}$		1769(1)	1772.0
C-1	$(2s^22p^2_{1/2})_0$	$(2s_{1/2}2p^2_{1/2}2p_{3/2})_1$	1802.0(8)	1801(2)	1804.4
O-1	$(2s^22p^2_{1/2}2p^2_{3/2})_2$	$(2s_{1/2}2p^2_{1/2}2p^3_{3/2})_2$		1806(2)	1808.8
O-3	$(2s^22p^2_{1/2}2p^2_{3/2})_0$	$(2s_{1/2}2p^2_{1/2}2p^3_{3/2})_1$	1829.0(9)		1833.3
N-1a	$(2s^22p^2_{1/2}2p_{3/2})_{3/2}$	$(2s_{1/2}2p^2_{1/2}2p^2_{3/2})_{1/2}$		1840(2)	1842.9
N-1b	$(2s^22p^2_{1/2}2p_{3/2})_{3/2}$	$(2s_{1/2}2p^2_{1/2}2p^2_{3/2})_{3/2}$		1842(2)	1844.7
F-1	$(2s^22p^2_{1/2}2p^3_{3/2})_{3/2}$	$(2s_{1/2}2p^2_{1/2}2p^4_{3/2})_{1/2}$	1866.5(5)	1871(2)	1870.7
O-2	$(2s^22p^2_{1/2}2p^2_{3/2})_2$	$(2s_{1/2}2p^2_{1/2}2p^3_{3/2})_1$	1890.8(5)	1891(2)	1894.0

Note: Experimental data from the measurements at SuperEBIT using the ECS X-ray calorimeter and the flat-crystal spectrometer. Theoretical energies from FAC. Units in eV. Table from [77].

like W^{43+} and Zn-like W^{44+}, which were not directly observed, were interpolated from the inferred Ge-like W^{42+} and Cu-like W^{45+} abundances. The 2000–2500 eV spectral interval contains a large number of transitions from several tungsten ions, of which the strongest are the $3d_{3/2}$–$4f_{5/2}$ transitions. As demonstrated in Fig. 2, these transitions can easily be resolved and individual charge states can be measured. The interval should therefore be suitable for measuring the tungsten charge balance in tokamak plasmas.

Of the M-shell tungsten ions, Ni-like W^{46+} is of special interest for moderately hot fusion plasmas. According to the charge-balance calculations by Pütterich et al., Ni-like W^{46+} will have a fractional abundance of more than 10% in the 3–7 keV electron temperature range [61]. This interval is what the ITER tokamak could be expected to run at during ohmic plasma operations. Ni-like W^{46+} has a ground configuration of $3s^23p^63d^{10}$ and therefore a relatively simple spectrum in low-density plasmas. The lowest excited levels are $(3d_{5/2}4s_{1/2})_{3,2}$, which can only decay to the ground state by magnetic octupole (M3) and electric quadrupole (E2) transitions, respectively. The first M3 transitions observed were in Ni-like Th^{62+} and Ni-like U^{64+} by Beiersdorfer et al. [62] at EBIT-I in 1991. The corresponding transition in mid-*Z* nickel-like ions has later been studied at Livermore by Träbert et al. [63–65]. The E2 and M3 transitions in nickel-like tungsten have attracted attention during the last few years. The two electric dipole (E1) forbidden transitions were first observed unresolved in the ASDEX Upgrade tokamak by Neu et al. in 1997 [14]. The feature was then interpreted as only the E2 transition, but the unexpected intensity of the line, which could not be explained by theory [16, 31, 61] prompted Loch et al. [66] and Ralchenko et al. [27, 67] to investigate if the feature could be a blend of the E2 and M3 transitions, similar to what was observed 15 years earlier in nickel-like uranium and thorium [62]. The wavelengths, or corresponding energy levels, of the two transitions have been calculated by a number of authors [27, 68–72]. The unresolved line has furthermore been observed at the NIST and Livermore EBIT facilities using X-ray calorimeters [27, 57].

The two nickel-like tungsten transitions have been resolved at SuperEBIT using crystal-spectrometer measurements [73]. A broad-band spectrometer [41] measured the two lines relative to K-shell lines from sodium and aluminum ions, which allowed the line positions of the E2 and M3 transitions to be determined to be 7.9280(6) and 7.9374(7) Å, respectively. A high-resolution crystal spectrometer [37] was also employed to fully resolve the two close-lying lines, and the line intensity ratios were studied at several electron-beam energies. The relative intensities turned out to vary very little with excitation energy. The relative polarization of the lines could also be studied using the two spectrometers. The polarization seems to depend only weakly on the excitation energy.

The unresolved M3–E2 line pair has previously been used to infer tungsten concentrations at ASDEX Upgrade in the 2.1–5.5 keV electron temperature interval [61, 74]. However, if the feature is resolved, it could also be used for electron-density and ion-temperature diagnostics. Electric dipole forbidden lines originating from metastable levels are often good diagnostics of electron densities, see e.g., [75] and [76]. The density dependences and population mechanisms of the M3 and E2 lines in nickel-like ions were first studied by Beiersdorfer et al. in 1991 [62]. Based on detailed collisional-radiative modeling, which included all singly excited levels with an $n = 3$ vacancy and an optical electron in the $n = 4$ or $n = 5$ shell, they showed that the intensity of the M3 line decreased with increasing electron density once a certain threshold was reached, while that of the neighboring E2 line increased with increasing density, keeping the combined intensity of the two transitions nearly constant. Their paper states that such forbidden lines are useful as diagnostic tools of the electron density of high-temperature plasmas. In the specific case of Ni-like W^{46+}, the density effect on the

M3 line was discussed by Loch et al. [66] and subsequently in more detail by Ralchenko [67], who also studied the density dependences of three other E1-forbidden lines in Ni-like W^{46+}, including the E2 transition. At Livermore, a new collisional-radiative model of nickel-like tungsten was very recently implemented in FAC, and the two lines were studied under various plasma conditions [73, 77]. Figure 3 shows how the relative intensities and profiles of the M3 and E2 lines change with temperatures (electron and ion temperatures are assumed equal) for two electron densities relevant to magnetic fusion plasmas. The line pair can be used for both electron-density measurements, based on the relative line intensities, as suggested by the previous work, and for ion-temperature measurements, inferred from the Doppler broadening of the line profiles.

At higher electron temperatures, the tungsten charge balance in a tokamak plasma will shift toward ions with 3s and 3p valence electrons. For these ions the strongest lines are $\Delta n = 0$ M-shell transitions. The line emissivities of Ca-like W^{54+} through Na-like W^{63+} have been calculated for $T_e = 20$ keV and shown to have several strong lines between 20 and 40 Å [77]. Whereas Ca-like W^{54+} through S-like W^{58+} ions have the strongest emission between 30 and 40 Å, the higher charge states dominate in the 20–25 Å interval. The presence of a large number of strong lines from many charge states in a rather narrow wavelength interval makes these spectra promising for plasma diagnostics. The relative abundances of Mg-like W^{62+} and Na-like W^{63+} ions between $T_e = 10$ and 30 keV (see Fig. 1) should make these charge states particularly interesting for diagnostics. The tungsten emission from a Maxwell–Boltzmann plasma has been calculated for three electron temperatures: 10, 20, and 30 keV (see Fig. 4). Included charge states range from Ca-like W^{54+} through Na-like W^{63+} with fractional abundances similar to Fig. 1. The line profiles are modeled with Gaussian distributions with linewidths corresponding to the Doppler broadening at each temperature.

Twenty $\Delta n = 0$ M-shell transitions from K-like W^{55+} through Ne-like W^{64+} ions have been measured in the 19–26 Å interval at SuperEBIT, using a high-resolution grazing-incidence instrument [78]. The $3s_{1/2}$–$3p_{3/2}$ resonance transitions in Na-like W^{63+} and Mg-like W^{62+} and the $3p_{1/2}$–$3d_{3/2}$ resonance transitions in Al-like W^{61+} and Si-like W^{60+} could be measured with an accuracy of 0.5 mÅ. Such precision makes the measurement useful for tests of large-scale atomic-structure calculations. The measured $3s_{1/2}$–$3p_{3/2}$ lines are compared with theoretical predictions in [77] and [78]. The experimental wavelengths for the Al-like W^{61+} and Si-like W^{60+} resonance lines are compared with the measured wavelengths from the NIST group [30] and calculated values from Huang [79, 80] and Safronova and Safronova [81] in Table 1. As noted by Kramida in these proceedings [82], the level designations for Al-like W^{61+} appear to be incorrect in [81]. The wavelength for the $(3s^2 3p_{1/2})_{1/2}$–$(3p_{3/2}^2 3s_{1/2})_{3/2}$ transition is therefore used for the comparison in Table 1.

4. L-shell tungsten spectroscopy

L-shell tungsten ions are proposed as the physics basis for the core imaging X-ray spectrometer (CIXS) that will diagnose ITER core plasmas [56, 83]. The instrument will mainly focus on neon-like tungsten, which is predicted to have a fractional abundance of more than 10% in the 12–33 keV temperature interval. The main objectives of the CIXS instrument are to measure the ion-temperature and rotational-velocity profiles of the ITER core plasmas using the Doppler effect. This requires the tungsten wavelengths to be accurately known. Previously, Ne-like W^{64+} was the only tungsten L-shell ion that had been studied in any detail. Several $n = 2$ to $n = 3$ wavelengths were measured by Beiersdorfer, using a high-resolution crystal spectrometer at EBIT-I [45]. Transitions from Si-like W^{60+} through Ne-like W^{64+} have also recently been measured by Biedermann et al. at the Berlin EBIT [17]. Biedermann et al. also observed radiative and dielectronic recombination lines from Si-like W^{60+} through N-like W^{67+} ions [17, 26]. Dielectronic recombination lines of Ne-like W^{64+} have also been studied at the Tokyo EBIT by Watanabe et al. [84].

Transitions from all the L-shell tungsten ions, i.e., Ne-like W^{64+} through Li-like W^{71+}, have been measured in Liver-

Fig. 6. Top: Theoretical tungsten spectra calculated at $n_e = 1 \times 10^{14}$ cm^{-3} for $T_e = 15$, 25, 35, and 45 keV. Strong lines are labeled according to charge state. Figure is adapted from [77]. Bottom: Experimental tungsten spectrum measured with the ECS X-ray calorimeter at SuperEBIT at an electron-beam energy of $E_b = 103$ keV. The lines are labeled according to Table 2.

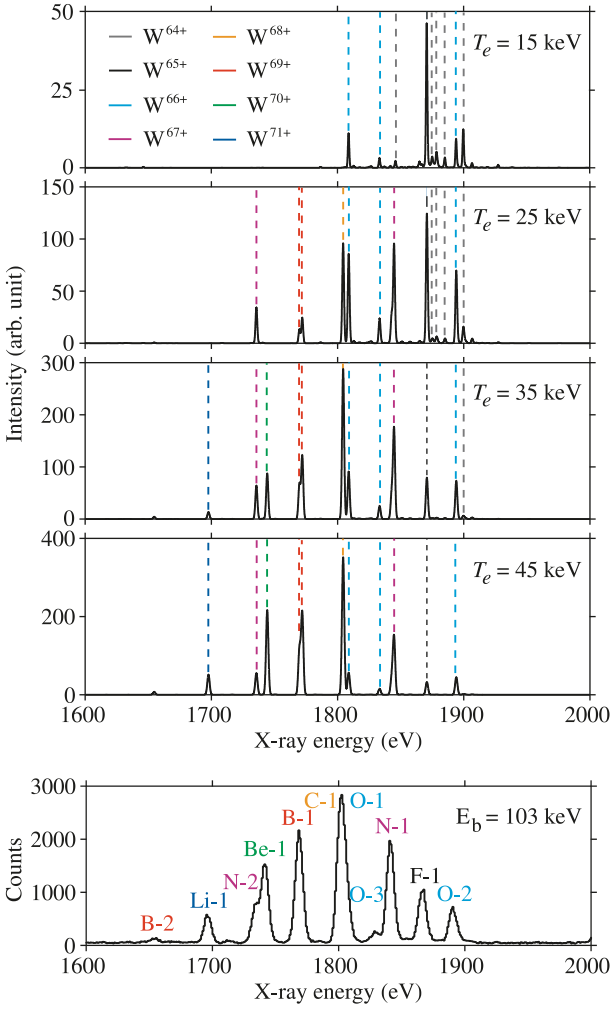

Table 3. Theoretical transition energies, transition probabilities and line emissivities of Ne-like W^{64+} calculated using FAC.

Line	Lower level	Upper level	ΔE (eV)	A (s^{-1})	ϵ (photon/s/ion)
M2	$(2s^22p^6)_0$	$(2s^22p^2_{1/2}2p^3_{3/2}3s_{1/2})_2$	8 293.4	4.12×10^9	90
3G	$(2s^22p^6)_0$	$(2s^22p^2_{1/2}2p^3_{3/2}3s_{1/2})_1$	8 302.0	1.50×10^{14}	339
E2L	$(2s^22p^6)_0$	$(2s^22p^2_{1/2}2p^3_{3/2}3p_{1/2})_2$	8 444.2	9.21×10^{11}	72
E2M	$(2s^22p^6)_0$	$(2s^22p^2_{1/2}2p^3_{3/2}3p_{3/2})_2$	8 834.6	9.22×10^{11}	17
3E	$(2s^22p^6)_0$	$(2s^22p^2_{1/2}2p^3_{3/2}3d_{3/2})_1$	8 990.1	7.84×10^{13}	31
3D	$(2s^22p^6)_0$	$(2s^22p^2_{1/2}2p^3_{3/2}3d_{5/2})_1$	9 120.6	2.88×10^{15}	732
3F	$(2s^22p^6)_0$	$(2s^22p_{1/2}2p^4_{3/2}3s_{1/2})_1$	9 683.8	3.65×10^{13}	51
3B	$(2s^22p^6)_0$	$(2s_{1/2}2p^63p_{1/2})_1$	10 316.8	6.81×10^{14}	81
3C	$(2s^22p^6)_0$	$(2s^22p_{1/2}2p^4_{3/2}3d_{3/2})_1$	10 404.0	1.49×10^{15}	231
3A	$(2s^22p^6)_0$	$(2s_{1/2}2p^63p_{3/2})_1$	10 705.9	4.55×10^{14}	44
4D	$(2s^22p^6)_0$	$(2s^22p^2_{1/2}2p^3_{3/2}4d_{5/2})_1$	11 950.9	9.77×10^{14}	101
4C	$(2s^22p^6)_0$	$(2s^22p_{1/2}2p^4_{3/2}4d_{3/2})_1$	13 295.4	6.31×10^{14}	39

Note: Emissivities are calculated for $n_e = 1 \times 10^{14}$ cm^{-3} and $T_e = 25$ keV. Table from [77].

more using SuperEBIT, employing both crystal and X-ray calorimeter spectrometers. There are two distinct groups of lines in L-shell spectra; the intrashell $n = 2$ to $n = 2$ transitions and the intershell $n = 2$ to $n = 3$ transitions. The intrashell transitions include the $2s_{1/2}$–$2p_{3/2}$ E1 transitions and the E1-forbidden $2p_{1/2}$–$2p_{3/2}$ transitions. A broad-band spectrum displaying both groups of lines is shown in Fig. 5. The $2s_{1/2}$–$2p_{3/2}$ transitions were measured with a flat-crystal spectrometer and were reported in [85]. The spectra were acquired when running SuperEBIT at an electron-beam energy of 103 keV, which allowed for the creation and excitation of ions up to Li-like W^{71+}. The flat-crystal spectrometer was equipped with an ADP crystal ($2d = 10.640$ Å), with a wide enough coverage to measure eleven transitions in the 1700 to 1900 eV interval. The line-position accuracies could be augmented by measurements made with the ECS spectrometer, which, although having a lower resolving power than the crystal spectrometer, achieved very good counting statistics. The ECS measured the intrashell lines at four electron-beam energies: $E_b = 23.5$, 51, 103, and 122 keV and allowed for better transition-energy values for six lines. In addition, six lines not observed with the crystal spectrometer could be measured, including some of the E1-forbidden $2p_{1/2}$–$2p_{3/2}$ transitions. The ECS spectrometer was energy calibrated with K-shell emission from hydrogen- and helium-like oxygen, aluminum, and argon ions. The transitions measured with the ECS X-ray calorimeter are presented in [77] and in Table 2, together with the values from the crystal spectrometer [85]. A spectrum displaying the $2s_{1/2}$–$2p_{3/2}$ transitions at $E_b = 103$ keV is shown in Fig. 6. The spectra were analyzed with the aid from theoretical spectra calculated using FAC (shown in [77]), and these transition energies are also listed in Table 2. Line F-1 was difficult to measure in the crystal data because of the possible blend with the He-like Si^{12+} line w. The influence of silicon in the ECS spectra is likely small. Nevertheless, the statistical uncertainty of the line position has been doubled to account for any small shifts. With the exception of F-1, all measured line positions determined from the two spectrometers agree within the experimental uncertainties.

Energy levels and transitions in ions isoelectronic to lithium and beryllium have been calculated by several authors. The experimental accuracy achieved for the resonance transitions in these one- and two-electron systems provide excellent testbeds for atomic theory. The measured line positions of the $2s_{1/2}$–$2p_{3/2}$ and the $(2s^2)_0$–$(2s_{1/2}2p_{3/2})_1$ transitions are listed in Table 1, together with some theoretical transition energies. Very good agreement is achieved with the predictions of Chen and Cheng [86] and Safronova et al. [87] for the beryllium-like resonance line and by Kim et al. [88] and Chen et al. [89] for the lithium-like tungsten line.

The tungsten $\Delta n = 0$ L-shell spectra have furthermore been modeled under fusion plasma conditions, as shown in Fig. 6. All the ions having fractional abundances above 1%, according to the charge-balance calculations presented in Fig. 1, were included in the calculations. The spectra are modeled for $n_e = 1 \times 10^{14}$ cm^{-3} at $T_e = 15$, 25, 35, and 45 keV. The ion temperatures are assumed equal to the electron temperatures, and the line profiles have been modeled with Gaussian functions having linewidths corresponding to the Doppler broadening. The width of a line at 1800 eV thus varies from 1.25 eV at $T_i = 15$ keV to 2.17 keV FWHM at $T_i = 45$ keV. The spectral signatures are strongly dependent on the electron temperature, and monitoring of this spectral interval could thus serve to determine the tungsten charge balance in tokamak plasmas. Note that the Maxwellian excitation functions for the modeled spectra differ from the mono-energetic excitation of the experimental EBIT spectrum also displayed in Fig. 6.

The ITER CIXS instrument will focus on the $n = 2$ to $n = 3$ transitions in neon-like tungsten and neighboring charge states. These transitions fall within the 8–12 keV spectral band. Ne-like W^{64+} has 36 singly excited $2l3l'$ energy levels, which give rise to a relatively simple spectrum. The two lowest excited levels are $(2p_{3/2}3s_{1/2})_{2,1}$, which decay to the ground state by a magnetic-quadrupole (M2) and electric-dipole (E1) transition, respectively. This system is hence the high-energy analog to the closed-shell nickel-like system, considered above. The neon-like spectrum has been calculated using FAC [77]. Calculated transition energies and transition probabilities are listed in Table 3, together with line emissivities for a $T_e = 25$ keV and $n_e = 1 \times 10^{14}$ cm^{-3} plasma.

The ECS X-ray calorimeter has acquired survey spectra of the 8–14 keV region at electron-beam energies of $E_b = 23.5$, 51, 103, and 122 keV. A spectrum from $E_b = 103$ keV is

Fig. 7. Experimental spectrum of $n = 2$ to $n = 3$ transitions in Na-like W^{63+} through Li-like W^{71+} ions, measured at SuperEBIT with the ECS X-ray calorimeter at an electron-beam energy of $E_b = 103$ keV. The spectrum has been divided in two parts for clarity. The lines are labeled according to charge state, except for the Ne-like W^{64+} lines, which are defined in Table 3. Fig. adapted from ref. 77.

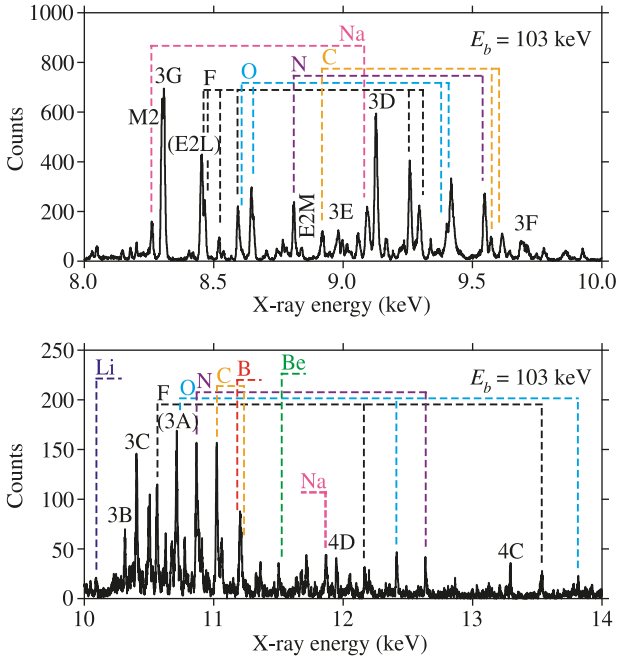

shown in Fig. 7, where lines from all the tungsten L-shell ions appear. The lines in Ne-like W^{64+} are identified based on FAC calculations, which are reported in [77] and in Table 3.

5. Summary

The Livermore WOLFRAM project has produced several spectroscopic measurements on M- and L-shell tungsten ions. The atomic physics of highly charged tungsten ions have been addressed by comparing high-precision wavelength and transition-energy measurements with theoretical predictions. Several spectral regions and transitions have been identified to be of interest for magnetic fusion diagnostics.

Current spectroscopic efforts at the Livermore EBIT facility include extreme ultraviolet measurements of few-times ionized tungsten, which are of interest for ITER divertor diagnostics, and further investigations of L-shell tungsten spectra in support of the ITER CIXS design.

Acknowledgments

This work was performed under the auspices of the United States Department of Energy by Lawrence Livermore National Laboratory under Contract No. DE-AC52–07NA-27344 and supported by LDRD project 09-ERD-016. The authors would like to acknowledge technical support from Ed Magee and helpful input from Dr. Alexander Kramida. Joel Clementson would like to acknowledge support from Professor Sune Svanberg, Dr. Sven Huldt, Dr. Christoph Biedermann, Professor Roger Hutton, Professor Claes-Göran Wahlström, and the late Professor Sveneric Johansson.

References

1. A.E. Kramida and T. Shirai. J. Phys. Chem. Ref. Data, **35**, 423 (2006). doi:10.1063/1.1836763.
2. A.E. Kramida and T. Shirai. At. Data Nucl. Data Tables, **95**, 305 (2009). doi:10.1016/j.adt.2008.12.002.
3. J.O. Ekberg, R. Kling, and W. Mende. Phys. Scr. **61**, 146 (2000). doi:10.1238/Physica.Regular.061a00146.
4. L. Iglesias, V. Kaufman, O. Garcia-Riquelme, and F.R. Rico. Phys. Scr. **31**, 173 (1985). doi:10.1088/0031-8949/31/3/004.
5. J. Sugar and V. Kaufman. Phys. Rev. A, **12**, 994 (1975). doi:10.1103/PhysRevA.12.994.
6. R.C. Isler, R.V. Neidigh, and R.D. Cowan. Phys. Lett. A, **63**, 295 (1977). doi:10.1016/0375-9601(77)90908-2.
7. E. Hinnov and M. Mattioli. Phys. Lett. A, **66**, 109 (1978). doi:10.1016/0375-9601(78)90010-5.
8. M. Finkenthal, L.L. Huang, S. Lippmann, H.W. Moos, P. Mandelbaum, J.L. Klapisch, and the TEXT Group. Phys. Lett. A, **127**, 255 (1988). doi:10.1016/0375-9601(88)90691-3.
9. J. Sugar, V. Kaufman, and W.L. Rowan. J. Opt. Soc. Am. B, **10**, 799 (1993). doi:10.1364/JOSAB.10.000799.
10. K. Asmussen, K.B. Fournier, J.M. Laming, R. Neu, J.F. Seely, R. Dux, W. Engelhardt, J.C. Fuchs, and the ASDEX Upgrade Team. Nucl. Fusion, **38**, 967 (1998). doi:10.1088/0029-5515/38/7/302.
11. A. Zigler, H. Zmora, N. Spector, M. Klapisch, J.L. Schwob, and A. Bar-Shalom. J. Opt. Soc. Am. **70**, 129 (1980). doi:10.1364/JOSA.70.000129.
12. P. Mandelbaum, M. Klapisch, A. Bar-Shalom, J.L. Schwob, and A. Zigler. Phys. Scr. **27**, 39 (1983). doi:10.1088/0031-8949/27/1/005.
13. N. Tragin, J.-P. Geindre, P. Monier, J.-C. Gauthier, C. Chenais-Popovics, J.-F. Wyart, and C. Bauche-Arnoult. Phys. Scr. **37**, 72 (1988). doi:10.1088/0031-8949/37/1/011.
14. R. Neu, K.B. Fournier, D. Schlögl, and J. Rice. J. Phys. At. Mol. Opt. Phys. **30**, 5057 (1997). doi:10.1088/0953-4075/30/21/036.
15. T. Pütterich, R. Neu, C. Biedermann, R. Radtke, and the ASDEX Upgrade Team. J. Phys. At. Mol. Opt. Phys. **38**, 3071 (2005). doi:10.1088/0953-4075/38/16/017.
16. R. Neu, R. Dux, A. Kallenback, T. Pütterich, M. Balden, J.C. Fuchs, A. Hermann, C.F. Maggi, M. O'Mullane, R. Pugno, I. Radivojevic, V. Rohde, A.C.C. Sips, W. Suttrop, and A. Whiteford and the ASDEX Upgrade Team. Nucl. Fusion, **45**, 209 (2005). doi:10.1088/0029-5515/45/3/007.
17. C. Biedermann, R. Radtke, R. Seidel, and T. Pütterich. Phys. Scr. **T134**, 014026 (2009). doi:10.1088/0031-8949/2009/T134/014026.
18. R. Causey, K. Wilson, T. Venhaus, and W.R. Wampler. J. Nucl. Mater. **266–269**, 467 (1999). doi:10.1016/S0022-3115(98)00538-8.
19. S.B. Utter, P. Beiersdorfer, and G.V. Brown. Phys. Rev. A, **61**, 030503 (2000). doi:10.1103/PhysRevA.61.030503.
20. S.B. Utter, P. Beiersdorfer, and E. Träbert. Can. J. Phys. **80**, 1503 (2002). doi:10.1139/p02-132.
21. P. Neill, C. Harris, A.S. Safronova, S. Hamasha, S. Hansen, U.I. Safronova, and P. Beiersdorfer. Can. J. Phys. **82**, 931 (2004). doi:10.1139/p04-053.
22. A.S. Safronova, V.L. Kantsyrev, P. Neill, U.I. Safronova, D.A. Fedin, N.D. Ouart, M.F. Yilmaz, G. Osborne, I. Shrestha, K. Williamson, T. Hoppe, C. Harris, P. Beiersdorfer, and S. Hansen. Can. J. Phys. **86**, 267 (2008). doi:10.1139/P07-170.
23. C. Biedermann, R. Radtke, J.L. Schwob, P. Mandelbaum, R. Doron, T. Fuchs, and G. Fußmann. Phys. Scr. T, **92**, 85 (2001).
24. R. Radtke, C. Biedermann, J.L. Schwob, P. Mandelbaum, and

R. Doron. Phys. Rev. A, **64**, 012720 (2001). doi:10.1103/PhysRevA.64.012720.
25. R. Radtke, C. Biedermann, P. Mandelbaum, and J.L. Schwob. J. Phys. Conf. Ser. **58**, 113 (2007). doi:10.1088/1742-6596/58/1/019.
26. C. Biedermann, R. Radtke, R. Seidel, and E. Behar. J. Phys. Conf. Ser. **163**, 012034 (2009). doi:10.1088/1742-6596/163/1/012034.
27. Y. Ralchenko, J.N. Tan, J.D. Gillaspy, J.M. Pomeroy, and E. Silver. Phys. Rev. A, **74**, 042514 (2006). doi:10.1103/PhysRevA.74.042514.
28. Y. Ralchenko, J. Reader, J.M. Pomeroy, J.N. Tan, and J.D. Gillaspy. J. Phys. At. Mol. Opt. Phys. **40**, 3861 (2007). doi:10.1088/0953-4075/40/19/007.
29. Y. Ralchenko, I.N. Draganic, J.N. Tan, J.D. Gillaspy, J.M. Pomeroy, J. Reader, U. Feldman, and G.E. Holland. J. Phys. At. Mol. Opt. Phys. **41**, 021003 (2008). doi:10.1088/0953-4075/41/2/021003.
30. J.D. Gillaspy, I.N. Draganić, Y. Ralchenko, J. Reader, J.N. Tan, J.M. Pomeroy, and S.M. Brewer. Phys. Rev. A, **80**, 010501 (2009). doi:10.1103/PhysRevA.80.010501.
31. R. Neu, K.B. Fournier, D. Bolshukhin, and R. Dux. Phys. Scr. T, **92**, 307 (2001).
32. M.A. Levine, R.E. Marrs, J.R. Henderson, D.A. Knapp, and M.B. Schneider. Phys. Scr. **T22**, 157 (1988). doi:10.1088/0031-8949/1988/T22/024.
33. M.A. Levine, R.E. Marrs, J.N. Bardsley, P. Beiersdorfer, C.L. Bennett, M.H. Chen, T. Cowan, D. Dietrich, J.R. Henderson, D.A. Knapp, A. Osterheld, B.M. Penetrante, M. B. Schneider, and J.H. Scofield. Nucl. Instrum. Methods Phys. Res., Sect. B, **43**, 431 (1989). doi:10.1016/0168-583X(89)90386-8.
34. R.E. Marrs. Can. J. Phys. **86**, 11 (2008). doi:10.1139/P07-110.
35. D.A. Knapp, R.E. Marrs, S.R. Elliott, E.W. Magee, and R. Zasadzinski. Nucl. Instrum. Methods Phys. Res. A, **334**, 305 (1993). doi:10.1016/0168-9002(93)90790-O.
36. P. Beiersdorfer and B.J. Wargelin. Rev. Sci. Instrum. **65**, 13 (1994). doi:10.1063/1.1144786.
37. P. Beiersdorfer, J.R. Crespo López-Urrutia, E. Förster, J. Mahiri, and K. Widmann. Rev. Sci. Instrum. **68**, 1077 (1997). doi:10.1063/1.1147791.
38. P. Beiersdorfer, J.R. Crespo López-Urrutia, P. Springer, S.B. Utter, and K.L. Wong. Rev. Sci. Instrum. **70**, 276 (1999). doi:10.1063/1.1149324.
39. P. Beiersdorfer, G.V. Brown, R. Goddard, and B.J. Wargelin. Rev. Sci. Instrum. **75**, 3720 (2004). doi:10.1063/1.1781754.
40. P. Beiersdorfer, E.W. Magee, E. Träbert, H. Chen, K. Lepson, M.F. Gu, and M. Schmidt. Rev. Sci. Instrum. **75**, 3723 (2004). doi:10.1063/1.1779609.
41. G.V. Brown, P. Beiersdorfer, and K. Widmann. Rev. Sci. Instrum. **70**, 280 (1999). doi:10.1063/1.1149339.
42. F.S. Porter, P. Beiersdorfer, G.V. Brown, M.F. Gu, R.L. Kelley, S. Kahn, C. Kilbourne, and D.B. Thorn. J. Phys. Conf. Ser. **163**, 012105 (2009). doi:10.1088/1742-6596/163/1/012105.
43. C.K. Stahle, D. McCammon, and K.D. Irwin. Phys. Today, **52**, 32 (1999). doi:10.1063/1.882776.
44. G.V. Brown, P. Beiersdorfer, J. Clementson, J. Dunn, R.L. Kelley, C.A. Kilbourne, M. Leutenegger, E. Magee, J. Park, F.S. Porter, M. Schneider, and E. Träbert. Society of photo-optical instrumentation engineers (SPIE) Conference Series. Vol. 7732. 2010. p. 77324Q.
45. P. Beiersdorfer. AIP Conf. Proc., **274**, 365 (1993). doi:10.1063/1.43681.
46. S.R. Elliott, P. Beiersdorfer, B.J. MacGowan, and J. Nilsen. Phys. Rev. A, **52**, 2689 (1995). doi:10.1103/PhysRevA.52.2689. PMID:9912550.
47. P. Beiersdorfer, S.R. Elliott, B.J. MacGowan, and J. Nilsen. AIP Conf. Proc., **332**, 512 (1995). doi:10.1063/1.47981.
48. J. Clementson, P. Beiersdorfer, M.F. Gu, H.S. McLean, and R.D. Wood. J. Phys. Conf. Ser. **130**, 012004 (2008). doi:10.1088/1742-6596/130/1/012004.
49. J. Clementson, P. Beiersdorfer, E.W. Magee, H.S. McLean, and R.D. Wood. J. Phys. At. Mol. Opt. Phys. **43**, 144009 (2010). doi:10.1088/0953-4075/43/14/144009.
50. M.L. Reinke, P. Beiersdorfer, N.T. Howard, E. Magee, Y. Podpaly, J.E. Rice, and J.L. Terry. Rev. Sci. Instrum. **81**, 10D736 (2010). doi:10.1063/1.3494380. PMID:21033927.
51. Y. Podpaly, J.E. Rice, P. Beiersdorfer, M.L. Reinke, J. Clementson, and H.S. Barnard. Can. J. Phys. **89**, 591 (2011). doi:10.1139/p11-038..
52. J. Clementson, P. Beiersdorfer, A.L. Roquemore, C.H. Skinner, D.K. Mansfield, K. Hartzfeld, and J.K. Lepson. Rev. Sci. Instrum. **81**, 10E326 (2010). doi:10.1063/1.3499607. PMID:21034024.
53. M.F. Gu. Can. J. Phys. **86**, 675 (2008). doi:10.1139/P07-197.
54. U.I. Safronova, A.S. Safronova, and P. Beiersdorfer. At. Data Nucl. Data Tables, **95**, 751 (2009). doi:10.1016/j.adt.2009.04.001.
55. U.I. Safronova, A.S. Safronova, and P. Beiersdorfer. J. Phys. At. Mol. Opt. Phys. **42**, 165010 (2009). doi:10.1088/0953-4075/42/16/165010.
56. P. Beiersdorfer, J. Clementson, J. Dunn, M.F. Gu, K. Morris, Y. Podpaly, E. Wang, M. Bitter, R. Feder, K.W. Hill, D. Johnson, and R. Barnsley. J. Phys. At. Mol. Opt. Phys. **43**, 144008 (2010). doi:10.1088/0953-4075/43/14/144008.
57. J. Clementson, P. Beiersdorfer, G.V. Brown, and M.F. Gu. Phys. Scr. **81**, 015301 (2010). doi:10.1088/0031-8949/81/01/015301.
58. F.S. Porter, P. Beiersdorfer, G.V. Brown, W. Doriese, J. Gygax, R.L. Kelley, C.A. Kilbourne, J. King, K. Irwin, C. Reintsema, and J. Ullom. J. Low Temp. Phys. **151**, 1061 (2008). doi:10.1007/s10909-008-9788-4.
59. G.V. Brown, J.S. Adams, P. Beiersdorfer, J. Clementson, M. Frankel, S.M. Kahn, R.L. Kelley, C.A. Kilbourne, D. Koutroumpa, M. Leutenegger, F.S. Porter, D.B. Thorn, and E. Träbert. AIP Conf. Proc., **1185**, 446 (2009). doi:10.1063/1.3292374.
60. F.S. Porter, J.S. Adams, P. Beiersdorfer, G.V. Brown, J. Clementson, M. Frankel, S.M. Kahn, R.L. Kelley, and C.A. Kilbourne. AIP Conf. Proc., **1185**, 454 (2009). doi:10.1063/1.3292376 .
61. T. Pütterich, R. Neu, R. Dux, A.D. Whiteford, M.G. O'Mullane, and the ASDEX Upgrade Team Team. Plasma Phys. Contr. Fusion, **50**, 085016 (2008). doi:10.1088/0741-3335/50/8/085016.
62. P. Beiersdorfer, A.L. Osterheld, J. Scofield, B. Wargelin, and R.E. Marrs. Phys. Rev. Lett. **67**, 2272 (1991). doi:10.1103/PhysRevLett.67.2272. PMID:10044384.
63. E. Träbert, P. Beiersdorfer, G.V. Brown, S. Terracol, and U.I. Safronova. Nucl. Instrum. Methods Phys. Res. B, **235**, 23 (2005). doi:10.1016/j.nimb.2005.03.138.
64. E. Träbert, P. Beiersdorfer, G.V. Brown, K. Boyce, R.L. Kelley, C.A. Kilbourne, F.S. Porter, and A. Szymkowiak. Phys. Rev. A, **73**, 022508 (2006). doi:10.1103/PhysRevA.73.022508.
65. E. Träbert, P. Beiersdorfer, and G.V. Brown. Phys. Rev. Lett. **98**, 263001 (2007). doi:10.1103/PhysRevLett.98.263001. PMID:17678086.

66. S.D. Loch, M.S. Pindzola, C.P. Balance, D.C. Griffin, A.D. Whiteford, and T. Pütterich. AIP Conf. Proc., **1185**, 233 (2006). doi:10.1063/1.2402775.
67. Y. Ralchenko. J. Phys. At. Mol. Opt. Phys. **40**, F175 (2007). doi:10.1088/0953-4075/40/11/F01.
68. H.L. Zhang, D.H. Sampson, and C.J. Fontes. At. Data Nucl. Data Tables, **48**, 91 (1991). doi:10.1016/0092-640X(91)90024-X.
69. K.B. Fournier. At. Data Nucl. Data Tables, **68**, 1 (1998). doi:10.1006/adnd.1997.0756.
70. K.M. Aggarwal, P.H. Norrington, K.L. Bell, F.P. Keenan, G.J. Pert, and S.J. Rose. At. Data Nucl. Data Tables, **74**, 157 (2000). doi:10.1006/adnd.1999.0827.
71. U.I. Safronova, A.S. Safronova, S.M. Hamasha, and P. Beiersdorfer. At. Data Nucl. Data Tables, **92**, 47 (2006). doi:10.1016/j.adt.2005.09.001.
72. C.P. Ballance and D.C. Griffin. J. Phys. At. Mol. Opt. Phys. **39**, 3617 (2006). doi:10.1088/0953-4075/39/17/017.
73. J. Clementson, P. Beiersdorfer, and M.F. Gu. Phys. Rev. A, **81**, 012505 (2010). doi:10.1103/PhysRevA.81.012505.
74. T. Pütterich, R. Neu, R. Dux, and the ASDEX Upgrade Team. 34th EPS Conference on Plasma Physics. Europhysics Conference Abstracts, Vol. 31F. pp. P–5.103.
75. R.W.P. McWhirter. Phys. Rep. **37**, 165 (1978). doi:10.1016/0370-1573(78)90040-6.
76. R. Mewe. Astron. Astrophys. Rev. **3**, 127 (1991). doi:10.1007/BF00873539.
77. J. Clementson. Ph.D. thesis. Lund University. 2010.
78. J. Clementson and P. Beiersdorfer. Phys. Rev. A, **81**, 052509 (2010). doi:10.1103/PhysRevA.81.052509.
79. K.N. Huang. At. Data Nucl. Data Tables, **32**, 503 (1985). doi:10.1016/0092-640X(85)90022-1.
80. K.N. Huang. At. Data Nucl. Data Tables, **34**, 1 (1986). doi:10.1016/0092-640X(86)90008-2.
81. U.I. Safronova and A.S. Safronova. J. Phys. At. Mol. Opt. Phys. **43**, 074026 (2010). doi:10.1088/0953-4075/43/7/074026.
82. A.E. Kramida. Can. J. Phys. **89**, 551 (2011). doi:10.1139/p11-045..
83. P. Beiersdorfer, G.V. Brown, J. Clementson, J. Dunn, K. Morris, E. Wang, R.L. Kelley, C.A. Kilbourne, F.S. Porter, M. Bitter, R. Feder, K.W. Hill, D. Johnson, and R. Barnsley. Rev. Sci. Instrum. **81**, 10E323 (2010). doi:10.1063/1.3495789. PMID:21034021.
84. H. Watanabe, N. Nakamura, D. Kato, T. Nakano, and S. Ohtani. Plasma Fusion Res. **2**, 027 (2007). doi:10.1585/pfr.2.027.
85. Y. Podpaly, J. Clementson, P. Beiersdorfer, J. Willaimson, G. V. Brown, and M.F. Gu. Phys. Rev. A, **80**, 052504 (2009). doi:10.1103/PhysRevA.80.052504.
86. M.H. Chen and K.T. Cheng. Phys. Rev. A, **55**, 166 (1997). doi:10.1103/PhysRevA.55.166.
87. M.S. Safronova, W.R. Johnson, and U.I. Safronova. Phys. Rev. A, **53**, 4036 (1996). doi:10.1103/PhysRevA.53.4036. PMID:9913369.
88. Y.-K. Kim, D.H. Baik, P. Indelicato, and J.P. Desclaux. Phys. Rev. A, **44**, 148 (1991). doi:10.1103/PhysRevA.44.148. PMID:9905666.
89. M.H. Chen, K.T. Cheng, W.R. Johnson, and J. Sapirstein. Phys. Rev. A, **52**, 266 (1995). doi:10.1103/PhysRevA.52.266. PMID:9912244.
90. U.I. Safronova, A.S. Safronova, and W.R. Johnson. J. Phys. At. Mol. Opt. Phys. **43**, 144001 (2010). doi:10.1088/0953-4075/43/14/144001.